

Digital Quantum Simulation of the Nonlinear Lindblad Master Equation Based on Quantum Trajectory Averaging

Yu-Guo Liu,¹ Heng Fan,^{1,2,3,4} and Shu Chen^{1,2,*}

¹*Beijing National Laboratory for Condensed Matter Physics,
Institute of Physics, Chinese Academy of Sciences, Beijing 100190, China*

²*School of Physical Sciences, University of Chinese Academy of Sciences, Beijing 100049, China*

³*Beijing Academy of Quantum Information Sciences, Beijing 100193, China*

⁴*Hefei National Laboratory, Hefei 230088, China*

(Dated: April 2, 2025)

Since precisely controlling dissipation in realistic environments is challenging, digital simulation of the Lindblad master equation (LME) is of great significance for understanding nonequilibrium dynamics in open quantum systems. However, achieving long-time simulations for complex systems with multiple dissipation channels remains a major challenge, both theoretically and experimentally. Here, we propose a 2-dilation digital simulation scheme for the non-linear Lindblad master equation (NLME) based on quantum trajectory averaging. The NLME continuously interpolates between full LME and the dynamical equation governed by the effective non-Hermitian Hamiltonian. Remarkably, for standard LMEs, our scheme reduces to a 1-dilation method that enables deterministic realizations without postselection. This deterministic nature overcomes a key limitation in some existing simulation methods, where repeated postselections lead to exponentially vanishing implementation probabilities. Consequently, our scheme allows efficient long-time simulations of LMEs with multiple jump operators. As a demonstration, we present numerical experiments simulating novel theoretical predictions in open quantum systems, including localization in open quantum systems and the postselected skin effect.

Introduction.— The Lindblad master equation (LME) plays a crucial role in the study of open quantum systems, providing a rigorous framework to describe the quantum system coupling with the environment under the Born-Markov approximation [1–3]. In recent years, the demand for precise control over dissipative processes has driven extensive theoretical efforts to explore novel nonequilibrium dynamical phenomena within the Lindblad framework, such as Liouvillian flat bands [4], postselected skin effects [5], and localization in open quantum systems [6, 7]. These studies often require carefully engineered dissipation operators, which are difficult to implement on analog simulation platforms. In contrast, digital quantum platforms provide a standardized and promising approach to simulation.

The primary challenge of digitally simulating the LME lies in implementing its intrinsically non-unitary nature using unitary logic gates. This difficulty can be addressed through approaches such as dilation methods [8–20], which effectively embed non-unitarity into enlarged unitary gates, and hybrid quantum-classical algorithms, including variational quantum simulation [22–25] and the quantum imaginary time evolution method [26, 27]. Currently, effective experimental schemes have been demonstrated for single-qubit and few-qubit systems [10, 12, 13, 17, 19–21, 27]. However, for large systems, numerous dissipation sources, and long-time evolution, significant theoretical and experimental challenges remain. For instance, the Stinespring dilation approach [8, 9] requires a large number of auxiliary qubits, potentially affecting its scalability. Moreover, if probabilistic approaches, such as Sz.-Nagy dilation (SND) [10–12], the linear combination of unitaries (LCU) method [13–15], and singular-value decomposition (SVD) method [16, 17] are used to iteratively simulate system evolution within each time step δt , the overall suc-

cess probability rapidly approaches zero as the number of time steps and dissipation sources increases.

An alternative simulation scheme for the LME on a classical computer is the quantum trajectory method [28–34], which interprets the LME as a stochastic average over individual trajectories of pure states. This approach significantly reduces memory usage, as it focuses on the state rather than the density matrix. Inspired by this method, Luo *et al.* [25] and Peng *et al.* [18] recently proposed new variational and dilation-based simulation schemes, which substantially reduce logical gate complexity. However, the former requires additional ansatz assumptions, while the latter remains a probabilistic implementation and still faces the challenge of an almost vanishing success probability at long times.

In our trajectory simulation scheme, we overcome the challenge of the overall success probability approaching zero. The key insight is to rigorously match the stochasticity in quantum trajectories with the probabilistic outcomes of measurements in quantum circuits. Each measurement outcome directly corresponds to a specific mathematical process in the quantum trajectory method: either a quantum jump or non-unitary evolution. Unlike methods based on SND, LCU, and SVD, where certain states are discarded after measurement, our approach ensures that every measurement outcome is meaningful.

Based on the principle of efficiently utilizing measurement randomness, our scheme can extend from deterministic trajectory simulations of the LME to probabilistic trajectory simulations of the non-linear Lindblad master equation (NLME) [5, 35–37]. The NLME describes the dynamics of an open system lacking an arbitrary proportion of quantum jumps, providing a continuous interpolation between the LME and the evolution of effective non-Hermitian Hamiltonian (ENHH). It gives a reasonable framework for study-

ing the interplay and competition between the non-Hermitian Hamiltonians and pure dissipation or pure measurement processes.

In this paper, we first introduce the trajectory-averaged interpretation of the NLME. Based on this interpretation, we propose a probabilistic 2-dilation implementation. For two special cases of the NLME, namely the LME and the ENHH, the scheme reduces to a 1-dilation. In particular, for the LME, the scheme becomes fully deterministic due to the absence of post-selection effects. Furthermore, we simulate a specific class of jump operators that are theoretically interesting but difficult to realize experimentally, demonstrating a numerical approach for simulating open-system localization and the postselected skin effect.

Trajectory-averaged interpretation of NLME.— The NLME is a generation of the LME [5, 35]. It continuously interpolates between LME and ENHH by reducing quantum jumps, given by

$$\begin{aligned} \frac{d}{dt}\rho &= \mathcal{L}_\eta(\rho) := -i[H, \rho] + \sum_{\mu=1}^M \mathcal{D}_\mu(\rho), \\ \mathcal{D}_\mu(\rho) &= \gamma_\mu \left(-\frac{1}{2} \{L_\mu^\dagger L_\mu, \rho\} + (1 - \eta_\mu) L_\mu \rho L_\mu^\dagger + \eta_\mu \langle L_\mu^\dagger L_\mu \rangle \rho \right), \end{aligned} \quad (1)$$

where the system with Hamiltonian H couples to the environment by M jump operators L_μ with strength γ_μ . The η_μ ($0 \leq \eta_\mu \leq 1$) is the postselection strength that calibrates the reduction ratio of quantum jumps. When $\eta_\mu = 0$ for all μ , the NLME reduces to the standard LME,

$$\frac{d\rho}{dt} = \mathcal{L}(\rho) := -i[H, \rho] + \sum_{\mu=1}^M \gamma_\mu \left(L_\mu \rho L_\mu^\dagger - \frac{1}{2} \{L_\mu^\dagger L_\mu, \rho\} \right). \quad (2)$$

Conversely, when $\eta_\mu = 1$ for all μ , the NLME simplifies to the evolution of ENHH,

$$\frac{d}{dt}\rho = -iH_{\text{eff}}\rho + i\rho H_{\text{eff}}^\dagger + \sum_{\mu=1}^M \gamma_\mu \langle L_\mu^\dagger L_\mu \rangle \rho, \quad (3)$$

where the ENHH takes the form $H_{\text{eff}} = H - \frac{i}{2} \sum_{\mu=1}^M \gamma_\mu L_\mu^\dagger L_\mu$.

The NLME can be interpreted by the quantum trajectory method [5]. The expectation value of an arbitrary observable \hat{O} is given by the average over many trajectories: $\langle \hat{O} \rangle = \text{Tr}(\hat{O}\rho) = \lim_{K \rightarrow \infty} \frac{1}{K} \sum_{i=1}^K \langle \phi_i(t) | \hat{O} | \phi_i(t) \rangle$. The quantum state at time $t + \delta t$ for the i -th trajectory is obtained from the state at time t through a stochastic evolution:

$$\begin{aligned} |\phi_i(t + \delta t)\rangle &= e^{-iH\delta t} \prod_{\mu=1}^M \mathcal{U}_\mu(\delta t) |\phi_i(t)\rangle, \\ \mathcal{U}_\mu(\delta t) &= \begin{cases} (1 - \eta_\mu)\delta p_\mu : & NL_\mu \\ 1 - (1 - \eta_\mu)\delta p_\mu : & \mathcal{N} \exp(-\frac{1}{2}\gamma_\mu L_\mu^\dagger L_\mu \delta t) \end{cases}, \end{aligned} \quad (4)$$

where \mathcal{N} denotes normalization process and $\delta p_\mu = \gamma_\mu \delta t \langle \phi_i(t) | L_\mu^\dagger L_\mu | \phi_i(t) \rangle$. The dissipation effect $\mathcal{U}_\mu(\delta t)$ represents

a stochastic process where the system either jumps to the state $\mathcal{N}L_\mu|\phi(t)\rangle$ with the probability of $(1 - \eta_\mu)\delta p_\mu$ or evolves to the state $\mathcal{N} \exp(-\frac{1}{2}\gamma_\mu L_\mu^\dagger L_\mu \delta t)|\phi(t)\rangle$.

Digital quantum simulation.— The key challenge in implementing an iterative simulation for a single quantum trajectory of NLME from Eq. (4) lies in how to realize the stochastic process $\mathcal{U}_\mu(\delta t)$. To address this within a quantum circuit, we assume a unitary gate U_μ that acts on the Hilbert space of the system along with two auxiliary qubits as follows:

$$U_\mu |00\rangle_a |\phi\rangle = |00\rangle_a C_\mu |\phi\rangle + |01\rangle_a B_\mu |\phi\rangle + |10\rangle_a A_\mu |\phi\rangle, \quad (5)$$

where the subscript a represents auxiliary qubits. After measuring the auxiliary qubits, the system probabilistically collapses into the state of $\mathcal{N}X_\mu|\phi\rangle$ ($X = A, B$, or C) with a probability of $\langle X_\mu^\dagger X_\mu \rangle := \langle \phi | X_\mu^\dagger X_\mu | \phi \rangle$.

To match the measurement outcomes of Eq. (5) with the stochastic results of $\mathcal{U}_\mu(\delta t)$, we assume that $A_\mu \propto \exp(-\frac{1}{2}\gamma_\mu L_\mu^\dagger L_\mu \delta t)$ and $B_\mu \propto L_\mu$. To precisely match their probabilities, we discard the $C_\mu|\phi\rangle$ state by postselecting the auxiliary qubits to not be in the $|00\rangle_a$ state, and require renormalized probability distribution to satisfy

$$\frac{\langle B_\mu^\dagger B_\mu \rangle}{\langle A_\mu^\dagger A_\mu \rangle + \langle B_\mu^\dagger B_\mu \rangle} = (1 - \eta_\mu)\delta p_\mu. \quad (6)$$

By enforcing both the probability constraint Eq. (6) and the unitarity condition $U_\mu^\dagger U_\mu = \mathbb{I}$, we obtain a solution for U_μ as

$$U_\mu = \begin{pmatrix} C_\mu & B_\mu & \tilde{A}_\mu & 0 \\ B_\mu & -C_\mu & 0 & \tilde{A}_\mu \\ A_\mu & 0 & -C_\mu^\dagger & -B_\mu^\dagger \\ 0 & A_\mu & -B_\mu^\dagger & C_\mu^\dagger \end{pmatrix}, \quad (7)$$

where

$$\begin{aligned} A_\mu &= \sqrt{1 - \gamma_\mu \delta t L_\mu^\dagger L_\mu}, \quad \tilde{A}_\mu = \sqrt{1 - \gamma_\mu \delta t L_\mu L_\mu^\dagger}, \\ B_\mu &= \sqrt{(1 - \eta_\mu)\gamma_\mu \delta t} L_\mu, \quad C_\mu = \sqrt{\eta_\mu \gamma_\mu \delta t} L_\mu, \end{aligned} \quad (8)$$

and note that $\exp(-\frac{1}{2}\gamma_\mu L_\mu^\dagger L_\mu \delta t) = A_\mu + \mathcal{O}(\delta t)$.

The 2-dilation method for realizing the full trajectory is presented in Fig. 1(a). The system and auxiliary qubits are initialized in the state $|\phi_i(0)\rangle$ and $|00\rangle_a$. Then, N iterations are carried out for a time evolution of duration $T = N\delta t$. During each time step δt , the unitary evolution governed by the system Hamiltonian is encoded in the logic gate $U_0 = e^{-iH\delta t}$. Each dissipation effect $\mathcal{U}_\mu(\delta t)$ is implemented by measuring and post-selecting the auxiliary qubits after applying the 2-dilation logic gate U_μ in Eq. (7), where only the measurement outcomes of $|01\rangle_a$ and $|10\rangle_a$ are considered valid. If the outcome is $|00\rangle_a$ the iteration is ended, and this trajectory is discarded. Following postselection, the auxiliary qubits are reset to $|00\rangle_a$ state in preparation for the next gate $U_{\mu+1}$.

Since the postselection requires that the measurement outcome $|00\rangle_a$ cannot appear throughout the entire trajectory, the

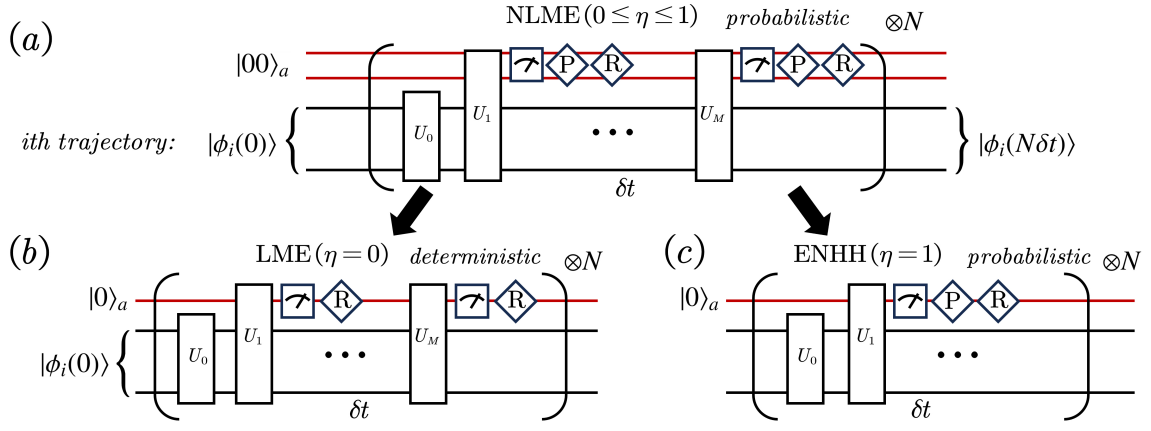


FIG. 1. Scheme of the quantum trajectory simulation: (a) the 2-dilation method for the NLME as Eq. (1), (b) the 1-dilation method for the LME as Eq. (2), and (c) the 1-dilation method for the evolution of ENHH as Eq. (3). The system is initialized in state $|\phi(0)\rangle$. The auxiliary qubits are initialized in state $|00\rangle_a$ in (a) and in state $|0\rangle_a$ in both (b) and (c). At each time step δt , the operations inside the brackets are executed. The gate $U_0 = e^{-iH\delta t}$ represents the evolution from system Hamiltonian. The gate $U_{\mu \geq 1}$, corresponding to the μ -th dissipation source, is given by Eq. (7) in (a), Eq. (11) in (b), and Eq. (12) in (c). After each measurement of auxiliary qubit, the postselection, denoted by 'P', is required only in (a) and (c), making their realization probabilistic. In contrast, the method in (b) is deterministic as it does not require postselection. In all three cases, the auxiliary qubit must be repeatedly reset to its initial state, denoted by 'R'.

success probability for a single trajectory, with M dissipation sources and $N\delta t$ time duration, is

$$P = \prod_{i=\delta t}^{N\delta t} \prod_{\mu=1}^M \left(1 - \langle \phi(t) | C_\mu^\dagger C_\mu | \phi(t) \rangle\right) \quad (9)$$

$$= \prod_{i=\delta t}^{N\delta t} \prod_{\mu=1}^M \left(1 - \eta_\mu \gamma_\mu \delta t \langle \phi(t) | L_\mu^\dagger L_\mu | \phi(t) \rangle\right).$$

P is roughly estimated as $(1 - \bar{\eta}\bar{\gamma}\langle L_\mu^\dagger L_\mu \rangle \delta t)^{NM}$, where $\bar{\eta} = \frac{1}{M} \sum_{\mu=1}^M \eta_\mu$ and $\bar{\gamma} = \frac{1}{M} \sum_{\mu=1}^M \gamma_\mu$.

When $\eta_\mu = 0$ for all μ , the NLME reduces to the standard LME in Eq. (2). At the same time, $C_\mu = 0$ and postselection success probability reaches unity, i.e., $P = 1$ in Eq. (9), which indicates that the 2-dilation probabilistic implementation of the NLME can reduce to the 1-dilation deterministic implementation of the LME, as shown in Fig. 1(b). Note that it does not require postselection because the stochasticity in $\mathcal{U}_\mu(t)$ is completely equivalent to the randomness of measurement outcomes. This means that after measuring the auxiliary qubit in the state

$$U_\mu |0\rangle_a |\phi\rangle = |0\rangle_a B_\mu |\phi\rangle + |1\rangle_a A_\mu |\phi\rangle, \quad (10)$$

where U_μ reduces to

$$U_\mu = \begin{pmatrix} B_\mu & \tilde{A}_\mu \\ A_\mu & -B_\mu^\dagger \end{pmatrix}, \quad (11)$$

if the outcome is $|1\rangle_a$, the system has an evolution of $\mathcal{N} \exp(-\frac{1}{2}\gamma_\mu L_\mu^\dagger L_\mu \delta t)$ by the A_μ , whereas the outcome of $|0\rangle_a$ corresponds to a quantum jump on the trajectory by the B_μ . The consistency of the probabilities between \mathcal{U}_μ and measurement outcomes is guaranteed by the constraint equation Eq. (6).

When $\eta_\mu = 1$ for all μ , the 2-dilation method for the NLME can also reduce to the 1-dilation method for the ENHH in Eq. (3) due to $B_\mu = 0$, as shown in Fig. 1(c). The gate U_μ and its action reduce to

$$U_\mu |0\rangle_a |\phi\rangle = |0\rangle_a C_\mu |\phi\rangle + |1\rangle_a A_\mu |\phi\rangle; \quad U_\mu = \begin{pmatrix} C_\mu & \tilde{A}_\mu \\ A_\mu & -C_\mu^\dagger \end{pmatrix}. \quad (12)$$

The postselection discards trajectories where the auxiliary qubit collapses to $|0\rangle_a$ after measurement.

Numerical experiments.— We first simulate a two-level atom with monitoring its spontaneous emission [5, 45] to demonstrate the validity of our scheme. The dynamic equation is

$$\frac{d}{dt}\rho = -iJ[\sigma^x, \rho] + \gamma \left(-\frac{1}{2} \{\sigma^+ \sigma^-, \rho\} + (1-\eta)\sigma^- \rho \sigma^+ + \eta \langle \sigma^+ \sigma^- \rangle \rho \right), \quad (13)$$

where σ^\pm is the spin raising and lowering operators and $\sigma^x = \sigma^+ + \sigma^-$. This NLME can be exactly solved by the vectorization method [5, 45]. We compare the evolution of excited-state probability from the exact solution with that from the digital simulation of our 2-dilation and 1-dilation methods in Fig. 1, where the curves exhibit good consistency.

The fundamental mission of quantum simulation is to explore complex systems. Now, we focus on a many-particle problem in an L -site open chain, with the evolution equation

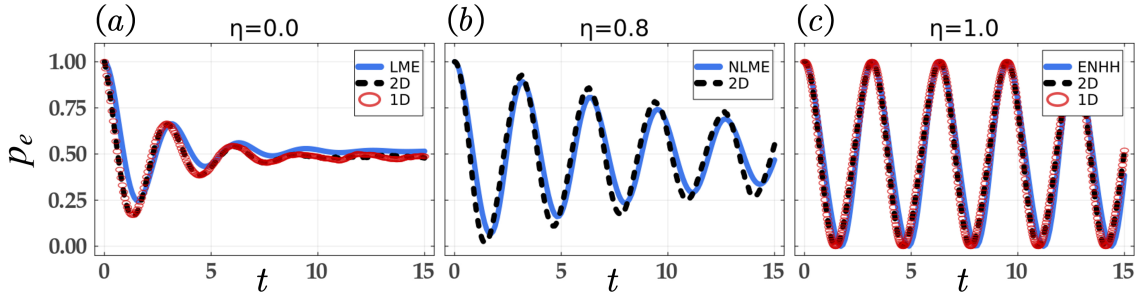


FIG. 2. The excited-state probability P_e of a spontaneously emitting two-level atom under different postselection strength η . The dynamic equation is given by Eq. (S2), with $J = 1$ and $\gamma = 0.5$ in all subplots, and $\eta = 0, 0.8, 1$ in (a), (b), and (c), respectively. The blue solid line represents the exact result obtained using vectorization method [4, 45]. The black dots and the red circles denote the results from the 2-dilation and 1-dilation method, respectively, with $\delta t = 0.01$ and an average over 5000 trajectories.

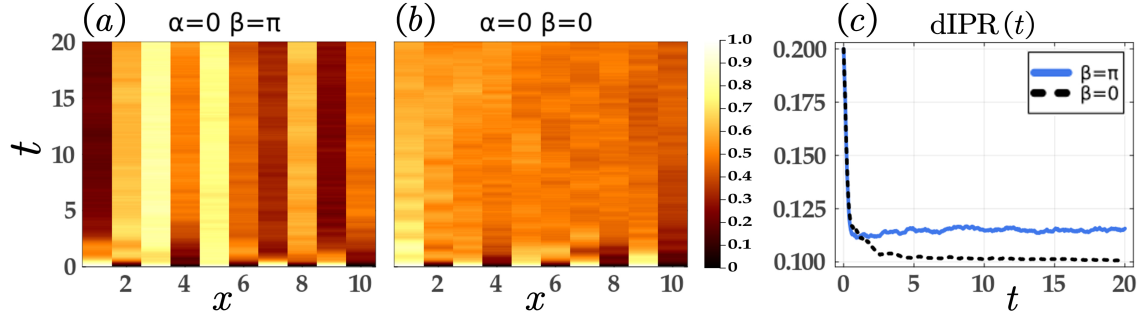


FIG. 3. Simulation of localization and thermalization in an open system. The probability distribution of the spin-up state in a 10-site chain evolves from the initial state $|\uparrow\uparrow\uparrow\cdots\downarrow\rangle$. The dynamics is governed by the LME in Eq. (14) with $J = 1$, $V = 2$, $\gamma = 1$ and $\eta = 0$. The jump operators take the form as Eq. (15) with $\alpha = 0$, $\beta = \pi$ in (a) and $\alpha = 0$, $\beta = 0$ in (b). We simulate the evolution by the 1-dilation method with $\delta t = 0.01$ and an average over 100 trajectories. The results show that the system is localized in (a) and thermalized in (b). The evolution curves of dIPR in both (a) and (b) are shown in (c).

given by:

$$\begin{aligned} \frac{d}{dt}\rho &= -i[H, \rho] + \gamma \sum_{l=1}^{L-1} \mathcal{D}_l(\rho), \\ H &= J \sum_{l=1}^{L-1} (\sigma_l^+ \sigma_{l+1}^- + \text{H.c.}) + \sum_{l=1}^L V \cos(2\pi\omega l) \sigma_l^z, \\ \mathcal{D}_l(\rho) &= -\frac{1}{2} \{L_l^\dagger L_l, \rho\} + (1 - \eta) L_l \rho L_l^\dagger + \eta \langle L_l^\dagger L_l \rangle \rho, \end{aligned} \quad (14)$$

where σ_l^μ ($\mu = z, +, -$) is the spin-1/2 operator at the site l , and $\omega = (\sqrt{5} - 1)/2$ indicates the quasicrystal potential. The local dissipation operator takes the following form:

$$L_l = \frac{1}{2} (\sigma_l^+ + e^{i\alpha} \sigma_{l+1}^+) (\sigma_l^- + e^{i\beta} \sigma_{l+1}^-), \quad (15)$$

which represents the phase-changing effect between neighboring spins. This kind of dissipation operator exhibits novel phenomena in theoretical studies, such as entangled state preparation [38–40], localization [6, 7], and the skin effect in open quantum systems [5, 41–43]. Note that this model is an intrinsic many-body evolution due to the $\hat{n}_l \hat{n}_{l+1}$ interaction ($\hat{n}_l := \sigma_l^+ \sigma_l^-$) existing in the evolution factor of $-\frac{1}{2} \gamma L_l^\dagger L_l \delta t$.

When $\alpha = 0$ and $\beta = \pi$, the L_l can induce the localization in standard LME ($\eta = 0$). We demonstrate it by our 1-dilation simulation of the evolution from the initial state $|\uparrow\uparrow\uparrow\downarrow\cdots\rangle$. As shown in Fig. 3(a), the probability distribution of the spin-up state, $\langle \hat{n}_l \rangle$, exhibits clear localization. As a comparison, in the case of $\alpha = \beta = 0$, the system fully thermalizes, as shown in Fig. 3(b). To quantify the difference between the two cases, we focus on the dynamic inverse participation ratio (dIPR) [44], $\text{dIPR}(t) = \sum_l \langle \hat{n}_l(t) \rangle^2 / [\sum_l \langle \hat{n}_l(t) \rangle]^2$, which is near $1/L$ for extended states and has a larger value for localized states. The curves of dIPR are shown in Fig. 3(c), where the value for $\beta = \pi$ is clearly larger than that for $\beta = 0$.

Furthermore, when $\alpha = \pi/2$, $\beta = -\pi/2$, $V = 0$, and $\eta \neq 0$, the steady state is expected to exhibit skin effect [5]. We simulate this postselected skin effect by our 2-dilation method in the supplementary materials [45].

Summary.— We tackle the scalability challenge in numerically simulating the LME over long-time evolutions with multiple dissipation sources. Based on quantum trajectory averaging, we propose a digital quantum simulation scheme for dynamics governed by the LME, ENHH, and NLME. The simulation of the NLME is achieved via a 2-dilation method, which simplifies to 1-dilation for the LME and ENHH. Notably,

our approach enables deterministic simulation of the standard LME without postselection, distinguishing it from existing probabilistic schemes and allowing for long-time simulations of complex open systems.

Our work paves the way for efficient digital quantum simulations of the LME, enables the exploration of the interplay between non-Hermitian Hamiltonians and pure dissipation processes through NLME simulations, and offers a promising simulation scheme for various cutting-edge theoretical models in open quantum systems and non-Hermitian physics.

Acknowledgments.— Y.-G. Liu thanks Zongsheng Zhou for the valuable discussions during the early stages of the work. The work is supported by National Key Research and Development Program of China (Grant Nos. 2021YFA1402104 and 2023YFA1406704), the National Natural Science Foundation of China (Grants Nos. 12474287, 12174436, T2121001, 92265207).

* schen@iphy.ac.cn

- [1] G. Lindblad, On the generators of quantum dynamical semigroups, *Commun.Math. Phys.* **48**, 119-130 (1976).
- [2] C. W. Gardiner and M. J. Collett, Input and output in damped quantum systems: Quantum stochastic differential equations and the master equation, *Phys. Rev. A* **31**, 3761 (1985).
- [3] D. Manzano, A short introduction to the Lindblad master equation, *AIP Advances* **10**, 025106 (2020).
- [4] Y.-G. Liu and S. Chen, Dynamical signatures of the Liouvillian flat band, *Phys. Rev. B* **107**, 134307 (2023).
- [5] Y.-G. Liu and S. Chen, Lindbladian dynamics with loss of quantum jumps, *Phys. Rev. B* **111**, 024303 (2025).
- [6] I. Yusipov, T. Laptjeva, S. Denisov, and M. Ivanchenko, Localization in Open Quantum Systems, *Phys. Rev. Lett.* **118**, 070402 (2017).
- [7] Y. Liu, Z. Wang, C. Yang, J. Jie and Y. Wang, Dissipation-Induced Extended-Localized Transition, *Phys. Rev. Lett.* **132**, 216301 (2024).
- [8] R. Cleve and C. Wang, Efficient quantum algorithms for simulating Lindblad evolution, in Proceedings of the 44th International Colloquium on Automata, Languages, and Programming, ICALP 2017 (Schloss Dagstuhl-Leibniz-Zentrum für Informatik GmbH, Dagstuhl Publishing, Dagstuhl, Germany, 2017).
- [9] Z. Ding, X. Li, and L. Lin, Simulating open quantum systems using Hamiltonian simulations, *PRX Quantum* **5**, 020332 (2024).
- [10] Z. Hu, R. Xia, and S. Kais, A quantum algorithm for evolving open quantum dynamics on quantum computing devices, *Sci. Rep.* **10**, 3301 (2020).
- [11] K. Head-Marsden, S. Krastanov, D.A. Mazziotti, and P. Narang, Capturing non-Markovian dynamics on near-term quantum computers, *Phys. Rev. Res.* **3**, 013182 (2021).
- [12] Z. Hu, K. Head-Marsden, D. A. Mazziotti, P. Narang, and S. Kais, A general quantum algorithm for open quantum dynamics demonstrated with the Fenna-Matthews-Olson complex, *Quantum* **6**, 726 (2022).
- [13] A. W. Schlimgen, K. Head-Marsden, L. M. Sager, P. Narang, and D. A. Mazziotti, Quantum Simulation of Open Quantum Systems Using a Unitary Decomposition of Operators, *Phys. Rev. Lett.* **127**, 270503 (2021).
- [14] A. W. Schlimgen, K. Head-Marsden, L. M. Sager, P. Narang, and D. A. Mazziotti, Quantum simulation of the Lindblad equation using a unitary decomposition of operators, *Phys. Rev. Res.* **4**, 023216 (2022).
- [15] N. Suri, J. Barreto, S. Hadfield, N. Wiebe, F. Wudarski, and J. Marshall, Two-Unitary Decomposition Algorithm and Open Quantum System Simulation, *Quantum* **7**, 1002 (2023).
- [16] A. W. Schlimgen, K. Head-Marsden, L. M. Sager-Smith, P. Narang, and D. A. Mazziotti, Quantum state preparation and nonunitary evolution with diagonal operators, *Phys. Rev. A* **106**, 022414 (2022).
- [17] E. K. Oh, T. J. Krogmeier, A. W. Schlimgen, K. Head-Marsden, Singular Value Decomposition Quantum Algorithm for Quantum Biology, *ACS Phys. Chem. Au* **4**, 393 (2024).
- [18] S. Peng, X. Sun, Q. Zhao, and H. Zhou, Quantum-Trajectory-Inspired Lindbladian Simulation, [arXiv:2408.10505 \[quant-ph\]](https://arxiv.org/abs/2408.10505).
- [19] L. Hu, X. Mu, W. Cai, Y. Ma, Y. Xu, H. Wang, Y. Song, C.-L. Zou, and L. Sun, Experimental repetitive quantum channel simulation, *Sci. Bull.* **63**, 1551 (2018).
- [20] J. Han, W. Cai, L. Hu, X. Mu, Y. Ma, Y. Xu, W. Wang, H. Wang, Y. P. Song, C.-L. Zou, and L. Sun, Experimental simulation of open quantum system dynamics via trotterization, *Phys. Rev. Lett.* **127**, 020504 (2021).
- [21] H. Lu, C. Liu, D.-S. Wang, L.-K. Chen, Z.-D. Li, X.-C. Yao, L. Li, N.-L. Liu, C.-Z. Peng, B. C. Sanders, Y.-A. Chen, and J.-W. Pan, Experimental quantum channel simulation, *Rev. A* **95**, 042310 (2017).
- [22] X. Yuan, S. Endo, Q. Zhao, Y. Li, and S. C. Benjamin, Theory of variational quantum simulation, *Quantum* **3**, 191 (2019).
- [23] S. Endo, J. Sun, Y. Li, S. C. Benjamin, and X. Yuan, Variational Quantum Simulation of General Processes, *Phys. Rev. Lett.* **125**, 010501 (2020).
- [24] M. Mahdian and H. D. Yeganeh, Hybrid quantum variational algorithm for simulating open quantum systems with near-term devices, *J. Phys. A: Math. Theor.* **53** 415301 (2020).
- [25] J. Luo, K. Lin, and X. Gao, Variational Quantum Simulation of Lindblad Dynamics via Quantum State Diffusion, *J. Phys. Chem. Lett.* **15**, 3516 (2024).
- [26] M. Motta, C. Sun, A. T. K. Tan, M. J. O'Rourke, E. Ye, A. J. Minnich, F. G. S. L. Brandão, and G. K.-L. Chan, Determining eigenstates and thermal states on a quantum computer using quantum imaginary time evolution, *Nat. Phys.* **16**, 205 (2020).
- [27] H. Kamakari, S.-N. Sun, M. Motta, and A. J. Minnich, Digital Quantum Simulation of Open Quantum Systems Using Quantum Imaginary-Time Evolution, *PRX Quantum* **3**, 010320 (2022).
- [28] J. Dalibard, Y. Castin, and K. Mølmer, Wave-function approach to dissipative processes in quantum optics, *Phys. Rev. Lett.* **68**, 580 (1992).
- [29] R. Dum, P. Zoller, and H. Ritsch, Monte Carlo simulation of the atomic master equation for spontaneous emission, *Phys. Rev. A* **45**, 4879 (1992).
- [30] R. Dum, A. S. Parkins, P. Zoller, and C. W. Gardiner, Monte Carlo simulation of master equations in quantum optics for vacuum, thermal, and squeezed reservoirs, *Phys. Rev. A* **46**, 4382 (1992).
- [31] K. Mølmer, C. Yvan, and D. Jean, Monte Carlo wavefunction method in quantum optics, *J. Opt. Soc. Am. B* **10**, 524 (1993).
- [32] M. B. Plenio and P. L. Knight, The quantum-jump approach to dissipative dynamics in quantum optics, *Rev. Mod. Phys.* **70**, 101 (1998).
- [33] A. J. Daley, Quantum trajectories and open many-body quan-

- tum systems, *Advances in Physics* **63**, 77 (2014).
- [34] H. M. Wiseman, Quantum state effusion, *J. Phys. A: Math. Theor.* **49** 411002 (2016).
- [35] P. Lewalle and K.-B. Whaley, Pontryagin-optimal control of a non-Hermitian qubit, *Phys. Rev. A* **107**, 022216 (2023).
- [36] M. Coppola, D. Karevski, and G. T. Landi, Conditional no-jump dynamics of noninteracting quantum chains, *Phys. Rev. B* **110**, 094315 (2024) .
- [37] A. Paviglianiti, G. D. Fresco, A. Silva, B. Spagnolo, D. Valenti, and A. Carollo, Breakdown of Measurement-Induced Phase Transitions Under Information Loss, [arXiv:2407.13837 \[quant-ph\]](https://arxiv.org/abs/2407.13837).
- [38] B. Kraus, H. P. Büchler, S. Diehl, A. Kantian, A. Micheli, and P. Zoller, Preparation of entangled states by quantum Markov processes, *Phys. Rev. A* **78**, 042307 (2008).
- [39] S. Diehl, A. Micheli, A. Kantian, B. Kraus, H. P. Büchler, and P. Zoller, Quantum states and phases in driven open quantum systems with cold atoms, *Nat. Phys.* **4**, 878 (2008) .
- [40] P. Schindler, M. Müller, D. Nigg, J. T. Barreiro, E. A. Martinez, M. Hennrich, T. Monz, S. Diehl, P. Zoller, and R. Blatt, Quantum simulation of dynamical maps with trapped ions, *Nat. Phys.* **9**, 361 (2013) .
- [41] Y.-P. Wang, C. Fang, and J. Ren, Absence of measurement-induced entanglement transition due to feedback-induced skin effect, *Phys. Rev. B* **110**, 035113 (2024).
- [42] X. Feng, S. Liu, S. Chen, and W. Guo, Absence of logarithmic and algebraic scaling entanglement phases due to the skin effect, *Phys. Rev. B* **107**, 094309 (2023).
- [43] Z.-C. Liu, K. Li, and Y. Xu, Dynamical Transition Due to Feedback-Induced Skin Effect, *Phys. Rev. Lett.* **133**, 090401 (2024) .
- [44] T. Li, Y.-S. Zhang, and W. Yi, Engineering dissipative quasicrystals, *Phys. Rev. B* **105**, 125111(2022).
- [45] See Supplemental Material for (i) the vectorization method and the digital simulation for two-level atom with monitoring spontaneous emission, (ii) the digital simulation of the postselection skin effect.

**SUPPLEMENTAL MATERIAL: DIGITAL QUANTUM SIMULATION OF THE NONLINEAR LINDBLAD MASTER EQUATION
BASED ON QUANTUM TRAJECTORY AVERAGING**

S1. Two-level atom with monitoring spontaneous emission

We introduce the vectorization method and the digital simulation for the model of two-level atom with monitoring spontaneous emission. Consider a spontaneously emitting two-level atom with the ground state $|g\rangle$ and excited state $|e\rangle$. Its dynamics is described by the LME,

$$\frac{d}{dt}\rho = -i[H, \rho] + \gamma \left(-\frac{1}{2}\{L^\dagger L, \rho\} + L\rho L^\dagger \right), \quad (\text{S1})$$

where $H = J\sigma^x$ is the driven Hamiltonian, $L = |g\rangle\langle e| = \sigma^-$ is the dissipative operator and γ is the spontaneous emission rate. The spontaneously emitted photons are monitored by an η -efficiency detector. In the postselection experiment, the observed data of atomic population is discarded when emission photons are detected simultaneously. With the remaining data, the evolution of atomic system is rebuilt by the NLME:

$$\frac{d}{dt}\rho = -iJ[\sigma^x, \rho] + \gamma \left(-\frac{1}{2}\{\sigma^+ \sigma^-, \rho\} + (1 - \eta)\sigma^- \rho \sigma^+ + \eta(\sigma^+ \sigma^-)\rho \right). \quad (\text{S2})$$

In the vectorization method, the density matrix ρ is mapped to the density vector $|\rho\rangle$:

$$\rho = \begin{pmatrix} \rho_{ee} & \rho_{eg} \\ \rho_{ge} & \rho_{gg} \end{pmatrix} \rightarrow |\rho\rangle = (\rho_{ee}, \rho_{eg}, \rho_{ge}, \rho_{gg})^T, \quad (\text{S3})$$

and the NLME is mapped as

$$\frac{d}{dt}|\rho\rangle = L_\eta |\rho\rangle, \quad (\text{S4})$$

where

$$L_\eta = -iH \otimes I + iI \otimes H^T - \frac{\gamma}{2}(L^\dagger L \otimes I + I \otimes L^T L^*) + (1 - \eta)\gamma L \otimes L^* + \eta\gamma \langle L^\dagger L \rangle, \quad (\text{S5})$$

where

$$H = \begin{pmatrix} 0 & J \\ J & 0 \end{pmatrix}, \quad L = \begin{pmatrix} 0 & 0 \\ 1 & 0 \end{pmatrix}, \quad I = \begin{pmatrix} 1 & 0 \\ 0 & 1 \end{pmatrix}. \quad (\text{S6})$$

Then we get the vectorized NLME:

$$\frac{d}{dt} \begin{pmatrix} \rho_{ee} \\ \rho_{eg} \\ \rho_{ge} \\ \rho_{gg} \end{pmatrix} = \begin{pmatrix} -iJ(\rho_{ge} - \rho_{eg}) + \eta\gamma\rho_{ee}^2 - \gamma\rho_{ee} \\ -iJ(\rho_{gg} - \rho_{ee}) + \eta\gamma\rho_{eg}\rho_{ee} - 0.5\gamma\rho_{eg} \\ iJ(\rho_{gg} - \rho_{ee}) + \eta\gamma\rho_{ge}\rho_{ee} - 0.5\gamma\rho_{ge} \\ iJ(\rho_{ge} - \rho_{eg}) + \eta\gamma\rho_{gg}\rho_{ee} + (1 - \eta)\gamma\rho_{ee} \end{pmatrix}, \quad (\text{S7})$$

which can be solved by the Runge-Kutta methods.

The scheme of digital simulation of Eq. (S6) is illustrated in Fig.1 in the main text. The 2-dilation method (Fig.1 (a)) is applicable for all values of η . Specifically, for $\eta = 0$ and $\eta = 1$, the simulation simplifies to the 1-dilation method, as shown in Fig.1 (b) and (c). We take the 2-dilation method as an example. We assume that the atom starts at the excited state, which is represented as the system qubit at the state $|\phi(0)\rangle = (1, 0)^T$. For each time step δt in a single trajectory simulation, we first apply the gate $U_0 = e^{-iJ\sigma^x\delta t}$ on $|\phi(t)\rangle$, followed by the gate U_1 on the state $|00\rangle_a \otimes U_0|\phi(t)\rangle$, where $|00\rangle_a = (1, 0, 0, 0)^T$ is a state of two auxiliary qubits and U_1 is given by Eq. (7) in the main text, with

$$\begin{aligned} A_1 &= \sqrt{1 - \gamma\delta t L^\dagger L} = \begin{pmatrix} \sqrt{1 - \gamma\delta t} & 0 \\ 0 & 1 \end{pmatrix} \\ \tilde{A}_1 &= \sqrt{1 - \gamma\delta t LL^\dagger} = \begin{pmatrix} 1 & 0 \\ 0 & \sqrt{1 - \gamma\delta t} \end{pmatrix} \\ B_1 &= \sqrt{(1 - \eta)\gamma\delta t} L = \begin{pmatrix} 0 & 0 \\ \sqrt{(1 - \eta)\gamma\delta t} & 0 \end{pmatrix} \\ C_1 &= \sqrt{\eta\gamma\delta t} L = \begin{pmatrix} 0 & 0 \\ \sqrt{\eta\gamma\delta t} & 0 \end{pmatrix}. \end{aligned} \quad (\text{S8})$$

We measure the auxiliary qubits and reset them to the state $|00\rangle_a$. Repeating the above steps N times results the state at the target time $|\phi(N\delta t)\rangle$. The postselection requires that in the N measurements, no outcomes should be $|00\rangle_a$; otherwise, this trajectory will be discarded. After multiple rounds of experiments, a sufficient number of valid trajectories are retained, and the desired simulation results can be obtained through valid trajectory averaging. Note that if $\eta = 0$, the measurement outcome of $|00\rangle_a$ is forbidden; therefore, all the trajectories are valid.

S2. Simulation of the postselected skin effect

Consider an L -site spin chain with the NLME,

$$\frac{d}{dt}\rho = -i[H, \rho] + \gamma \sum_{l=1}^{L-1} \left(-\frac{1}{2}\{L_l^\dagger L_l, \rho\} + (1-\eta)L_l\rho L_l^\dagger + \eta\langle L_l^\dagger L_l \rangle \rho \right), \quad (\text{S9})$$

where $H = J \sum_{l=1}^{L-1} (\sigma_l^+ \sigma_{l+1}^- + \text{H.c.})$ and

$$L_l = \frac{1}{2}(\sigma_l^+ + e^{i\alpha} \sigma_{l+1}^+)(\sigma_l^- + e^{i\beta} \sigma_{l+1}^-). \quad (\text{S10})$$

Note that the evolution from $\exp(-\frac{1}{2}\gamma L_l^\dagger L_l \delta t)$ indicates this model is an intrinsic many-body problem due to the $\hat{n}_l \hat{n}_{l+1}$ interaction ($\hat{n}_l := \sigma_l^+ \sigma_l^-$) existing in

$$L_l^\dagger L_l = \frac{1}{2} (\hat{n}_l + \hat{n}_{l+1} + e^{i\beta} \sigma_l^+ \sigma_{l+1}^- + e^{-i\beta} \sigma_{l+1}^+ \sigma_l^- + [\cos(\alpha + \beta) - 1] \hat{n}_l \hat{n}_{l+1}), \quad (\text{S11})$$

except for $\cos(\alpha + \beta) = 1$.

We simulate the dynamics by the 2-dilation method. The core gate U_l , corresponding to L_l , is given by

$$U_l = \begin{pmatrix} C_l & B_l & \tilde{A}_l & 0 \\ B_l & -C_l & 0 & \tilde{A}_l \\ A_l & 0 & -C_l^\dagger & -B_l^\dagger \\ 0 & A_l & -B_l^\dagger & C_l^\dagger \end{pmatrix}, \quad (\text{S12})$$

where all identity matrices outside the sites l and $l+1$ are omitted and

$$\begin{aligned} A_l &= \sqrt{1 - \gamma\delta t L_l^\dagger L_l} = \begin{pmatrix} \sqrt{1 - \gamma\delta t \cos^2(\frac{\alpha+\beta}{2})} & 0 & 0 & 0 \\ 0 & (1 + \sqrt{1 - \gamma\delta t})/2 & (\sqrt{1 - \gamma\delta t} - 1)e^{i\beta}/2 & 0 \\ 0 & (\sqrt{1 - \gamma\delta t} - 1)e^{-i\beta}/2 & (1 + \sqrt{1 - \gamma\delta t})/2 & 0 \\ 0 & 0 & 0 & 1 \end{pmatrix} \\ \tilde{A}_l &= \sqrt{1 - \gamma\delta t L_l L_l^\dagger} = \begin{pmatrix} \sqrt{1 - \gamma\delta t \cos^2(\frac{\alpha+\beta}{2})} & 0 & 0 & 0 \\ 0 & (1 + \sqrt{1 - \gamma\delta t})/2 & (\sqrt{1 - \gamma\delta t} - 1)e^{-i\alpha}/2 & 0 \\ 0 & (\sqrt{1 - \gamma\delta t} - 1)e^{i\alpha}/2 & (1 + \sqrt{1 - \gamma\delta t})/2 & 0 \\ 0 & 0 & 0 & 1 \end{pmatrix} \\ B_l &= \sqrt{(1 - \eta)\gamma\delta t} L_l = \frac{\sqrt{(1 - \eta)\gamma\delta t}}{2} \begin{pmatrix} 1 + e^{i(\alpha+\beta)} & 0 & 0 & 0 \\ 0 & 1 & e^{i\beta} & 0 \\ 0 & e^{i\alpha} & e^{i(\alpha+\beta)} & 0 \\ 0 & 0 & 0 & 0 \end{pmatrix} \\ C_l &= \sqrt{\eta\gamma\delta t} L_l = \frac{\sqrt{\eta\gamma\delta t}}{2} \begin{pmatrix} 1 + e^{i(\alpha+\beta)} & 0 & 0 & 0 \\ 0 & 1 & e^{i\beta} & 0 \\ 0 & e^{i\alpha} & e^{i(\alpha+\beta)} & 0 \\ 0 & 0 & 0 & 0 \end{pmatrix}. \end{aligned} \quad (\text{S13})$$

When $\alpha = \pi/2$, $\beta = \pi/2$, and $\eta \neq 0$, the steady state is expected to exhibit the postselected skin effect [5]. We simulate this dynamics of an 8-site chain from the initial state $|\uparrow\downarrow\uparrow\cdots\downarrow\rangle$. When $\eta = 0.4$, the postselection causes the probability distribution of the spin-up state to become concentrated toward the left, as shown in Fig. S1(a). As a comparison, in the case of $\eta = 0$, the

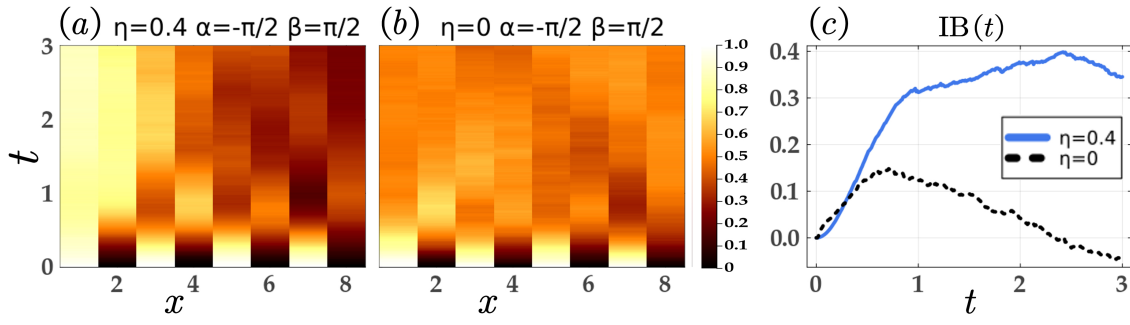


FIG. S1. Simulation of the postselected skin effect. The probability distribution of the spin-up state in an 8-site chain evolves from the initial state $|\uparrow\downarrow\uparrow\cdots\downarrow\rangle$. The dynamics is governed by the NLME in Eq. (14) with $J = 1$, $V = 0$, and $\gamma = 2$. The jump operators take the form of Eq. (15) with $\alpha = -\pi/2$, $\beta = \pi/2$. When postselection is applied, the spin-up state tends to move toward the left as shown in (a) with $\eta = 0.4$. As a comparison, for $\eta = 0$, the system is thermalized in (b). The results are simulated using the 2-dilation method with $\delta t = 0.01$ and an average over 90 valid trajectories for $\eta = 0.4$ and 100 trajectories for $\eta = 0$. The evolution curves of IB in both (a) and (b) are shown in (c).

system tends to thermalize, as shown in Fig. S1(b). To quantify the difference between the two cases, we define the imbalance between left and right part of the chain by

$$\text{IB}(t) = \left(\sum_{l=1}^{L/2} \langle \hat{n}_l(t) \rangle - \sum_{l=L/2+1}^L \langle \hat{n}_l(t) \rangle \right) / \left(\sum_{l=1}^L \langle \hat{n}_l(t) \rangle \right). \quad (\text{S14})$$

As shown in Fig. S1(c), the IB tends to 0 for $\eta = 0$ and $\text{IB} \neq 0$ for $\eta = 0.4$, which implies the postselected skin effect.

Additionally, we would like to mention that when $\eta \neq 0$, the simulation of the NLME is a probabilistic realization, which is still challenged by the success probability approaching zero. This is reflected in the fact that we obtain 90 valid trajectories from 300000 trials in the simulation for $\eta = 0.4$. However, the simulation of the standard LME is a deterministic realization. Therefore, we obtain 100 valid trajectories just 100 trials of simulation for $\eta = 0$